A Fast Alternative to the Galvanostatic Intermittent Titration Technique

Yu-Chuan Chien
Uppsala University https://orcid.org/0000-0003-4767-9471
Haidong Liu
Uppsala University
Ashok Menon
Uppsala University https://orcid.org/0000-0001-8148-8615
William Brant
Uppsala University https://orcid.org/0000-0002-8658-8938
Daniel Brandell (daniel.brandell@kemi.uu.se)
Uppsala University https://orcid.org/0000-0002-8019-2801
Matthew J. Lacey

Article

Keywords: galvanostatic intermittent titration technique (GITT) alternative, intermittent current interruption (ICI) method, diffusion coefficients

Posted Date: October 20th, 2021

DOI: https://doi.org/10.21203/rs.3.rs-960461/v1

A Fast Alternative to the Galvanostatic Intermittent Titration Technique

Yu-Chuan Chien[a], Haidong Liu[a], Ashok S. Menon[a], William R. Brant[a], Daniel Brandell[a,*], Matthew J. Lacey[b,*]

[a]Department of Chemistry—Ångström Laboratory, Uppsala University, Box 538, Lägerhyddsvägen 1, 751 21 Uppsala, Sweden

[b]Scania CV AB, 151 87 Södertälje, Sweden

Abstract

The galvanostatic intermittent titration technique (GITT) has been regarded as the go-to method for determining the diffusion coefficients of Li-ions in insertion electrode materials at various states of charge (SoC). However, the method is notoriously time-consuming. In this work, the intermittent current interruption (ICI) method, which has previously been employed to investigate the progression of internal resistances in Li-ion cells, is demonstrated to provide comparably accurate measurements of diffusion coefficients with a drastically reduced experimental time. Theoretically, it is first derived from Fick's laws that the ICI method renders essentially the same information as GITT. Experimentally, both GITT and ICI are then compared side-by-side in a three-electrode half-cell of $LiNi_{0.8}Mn_{0.1}Co_{0.1}O_2$ (NMC811). It is shown that the results from both methods match where the assumption of semi-infinite diffusion applies. Moreover, the benefit of the comparatively non-disruptive ICI method to *operando* characterization methods is demonstrated via correlation of changes in the continuously monitored diffusion coefficient of Li^+ in NMC811 to structural changes in the material by *operando* X-ray diffraction (XRD).

1 Introduction

As the demand for electrochemical energy storage surges, the research, development and application of new systems require comprehensive understanding of the electrochemical properties at an ever-increasing pace. A critical parameter for the community, from materials chemists to application engineers, is the diffusion coefficient of the charge carriers; i.e., Li^+, in the case of Li-ion batteries. The galvanostatic intermittent titration technique (GITT) has been the most widely applied method for deriving the diffusion coefficient from electrochemical measurements. Derived from Fick's second law, GITT was first demonstrated in 1977 for a bulk Li_3Sb electrode.[1] The technique consists of two repeating steps. First, a constant current is applied for a duration where the assumption of semi-infinite diffusion holds. Second, the current is switched off until the voltage becomes invariant, which indicates that equilibrium is

reached. Through the analysis of the electrode potential measured during the current pulse and the change in the equilibrium potential, GITT renders the chemical diffusion coefficient* of the charge-carrying ions. Later, the technique was applied to porous composite electrodes of Li-ion-insertion materials,[2] which is the format of the majority of electrodes in state-of-the-art Li-ion batteries. Despite practical issues due to the geometry of composite electrodes,[3] such as nonuniform current distribution, the technique serves as a powerful tool for the determination of diffusion coefficients if proper experimental parameters are chosen,[4,5] e.g. appropriate current and duration of the current pulses. In addition, more sophisticated methods of extracting the experimental parameters enhances the accuracy and applicability of the GITT,[4,5] for example, selecting the voltage response only from the semi-infinite diffusion and use linear regression to derive its slope.

However, the time required to perform a GITT measurement remains one major drawback. In order to reach the equilibrium condition, the test cell has to be relaxed substantially longer than the time spent on applying current.[5] This results in an experiment that can be anywhere from 8 to 100 times longer than a typical galvanostatic test cycle.[4,5] Although the test may be accelerated by increasing the duration of current pulses and selecting only the initial data points for the analysis[6] or introducing a constant potential step instead of the relaxation step,[7] these methods either reduce the number of measurements of diffusion coefficient or still require substantial amount of time. In addition, such a test protocol makes it difficult to couple GITT with simultaneous materials characterization, e.g. diffraction or spectroscopy, which can provide valuable structural and/or chemical information at the moment where the process under investigation takes place. In other words, the length of time needed for a typical GITT experiment essentially precludes its use in *operando* methods, and hence the coupling of *operando* methods with diffusion coefficient measurements.

In this work, an efficient and non-disruptive alternative to the GITT is proposed: the intermittent current interruption (ICI) method. Our group first developed the ICI method for characterizing the porous carbon electrodes in lithium–sulfur batteries,[8–10] and the method has more recently been applied more widely for different battery cell chemistries.[11–13] The method introduces transient current interruptions (usually 1 to 10 seconds) while the cell is under constant-current cycling. By analyzing the potential change during the current pauses,

* The difference between chemical and tracer diffusion coefficients is elaborated in the original GITT manuscript.[1] For simplicity, the former will be referred to as diffusion coefficient in the following text.

quantities describing the time-independent and time-dependent parts of the resistance can be derived, which are termed internal resistance and diffusion resistance coefficient, respectively.[10] With the porous electrode model,[14] it has been shown that the derived diffusion resistance coefficient is proportional to the coefficient of the Warburg element used when fitting electrochemical impedance spectra (EIS).[10] Since the Warburg element describes both the capacitive behavior in porous electrodes[14,15] and diffusion processes[16–18], it is a logical consequence that the ICI method can also characterize diffusion processes in an electrochemical system.

We here demonstrate mathematically that the ICI method can render the diffusion coefficient based on Fick's second law and requires much less experimental time than GITT. The theoretical derivations of GITT and ICI are elaborated and compared. Three-electrode cells of $LiNi_{0.8}Mn_{0.1}Co_{0.1}O_2$ (NMC811) are then tested following a protocol that enables the direct comparison of GITT, ICI and EIS. Finally, the combination of *operando* X-ray diffraction (XRD) and the ICI method is demonstrated to directly correlate the structural evolution to the Li-ion mobility. This example manifests not only the efficiency of the ICI method in probing the transport properties, but also its compatibility with *operando* techniques. Moreover, it also indicates the potential of the ICI method as a tool for state of heath estimation of Li-ion batteries.

2 Methodology

2.1 Derivation of GITT

The derivation of GITT starts from the solution to Fick's second law in one-dimension[1]:

$$\frac{\partial C(x,t)}{\partial t} = D\frac{\partial^2 C(x,t)}{\partial x^2} \qquad 1$$

where C is the concentration of the diffusing species, x is the position, t is time and D is the diffusion coefficient. The boundary conditions with an applied current $i(t)$ and an initial concentration C_0 are as follows:

$$\begin{cases} -D\dfrac{\partial C}{\partial x} = \dfrac{i(t)}{nFA} \\ C(x,0) = C_0 \end{cases} \qquad 2$$

where n is the charge number of the diffusing species (which is 1 for Li ion), F is the Faraday constant and A is the area of the surface where the diffusing

ions enter. For GITT, a constant current I is applied.

$$i(t) = I \tag{3}$$

With the above, $C(x,t)$ can be solved for planar diffusion[1] or spherical diffusion if transformed to the spherical coordinates,[4,19–22] which is detailed in Equation S3 in the Supporting Information (SI). In either case, when $t \ll L^2/D$, where L is the diffusion length or particle radius in the spherical case, semi-infinite diffusion can be assumed and the concentration at the surface can be expressed as:

$$C(0,t) = C_0 - \frac{2I\sqrt{t}}{FA\sqrt{D\pi}} \tag{4}$$

$$\frac{dC(0,t)}{d\sqrt{t}} = -\frac{2I}{FA\sqrt{D\pi}} \tag{5}$$

Supposing that the change in concentration is small and thus linear to the change in the potential E but in the opposite direction (i.e., the electrode potential increases with decreasing Li-ion concentration), the above expression can be expanded to:

$$\frac{dE}{d\sqrt{t}} = \frac{2I}{FA\sqrt{D\pi}}\frac{dE}{dC(0,t)} \tag{6}$$

With both derivatives of E extracted from experimental data, which will be elaborated in section 2.3, the diffusion coefficient can be calculated by reorganizing Equation 6.

$$D = \frac{4}{\pi}\left(\frac{I}{FA}\frac{\frac{dE}{dC(0,t)}}{\frac{dE}{d\sqrt{t}}}\right)^2 \tag{7}$$

2.2 Derivation of the ICI method

Instead of analyzing the potential change from open circuit to a constant current load, the ICI method utilizes the opposite case where the current is switched to zero from a constant current load. Considering a constant current I being applied from $t = 0$ and switched off at $t = \tau_1 > 0$, Equation 3 is changed to:

$$i(t) = I - IH(t) \tag{8}$$

where H is the Heaviside function, defined as:

$$H(t) = \begin{cases} 0, & t < \tau_1 \\ 1, & t \geq \tau_1 \end{cases} \tag{9}$$

By inserting Equation 8 into Equation 2 as the boundary conditions, Equation 1 can now be solved as the following by the Zero-Shift Theorem.[16]

$$C(0,t) = C_0 + F(t) - H(t)F(t-\tau_1) \quad 10$$

where $C_0 + F(t)$ is the full solution of Equation 1 when $i(t) = I$, shown in Equation S3. $F(t - \tau_1)$ can be approximated by the semi-infinite diffusion case ($t << L^2/D$) since the ICI method only analyzes the potential change in a short period Δt after the current is switched off, which means $\Delta t = t - \tau_1 << L^2/D$. Thus, when $t \geq \tau_1$, Equation 10 can be written as:

$$C(0,t) = C_0 - F(t) + \frac{2I\sqrt{t-\tau_1}}{FA\sqrt{D\pi}} \quad 11$$

So, the surface concentration at $t = \tau_1 + \Delta t$ is:

$$C(0,\tau_1+\Delta t) = C_0 - F(\tau_1+\Delta t) + \frac{2I\sqrt{\Delta t}}{FA\sqrt{D\pi}} \quad 12$$

Assuming that τ_1 is so much larger than Δt that $F(\tau_1+\Delta t) \approx F(\tau_1)$ and thus independent of Δt, which is a criterion for the ICI method and is discussed in the SI, the following is obtained:

$$\frac{dC(0,t)}{d\sqrt{\Delta t}} = \frac{2I}{FA\sqrt{D\pi}} \quad 13$$

This expression is similar to Equation 5 and if the change in concentration is small, it can be expanded to:

$$-\frac{dE}{d\sqrt{\Delta t}} = \frac{2I}{FA\sqrt{D\pi}}\frac{dE}{dC(0,t)} \quad 14$$

In the analysis of the ICI method,[9,10] which will be elaborated in section 2.4, $dE/d\sqrt{\Delta t}$ is readily obtained. How $dE/dC(0,t)$ can be obtained with the ICI method will be discussed in section 2.4. With both $dE/d\sqrt{t}$ and $dE/dC(0,t)$ obtainable from the ICI method, the diffusion coefficient can then be calculated from Equation 7.

2.3 Experimental execution of GITT

To employ Equation 7 in a conventional GITT measurement, the two derivatives of E (dE/dC and $dE/d\sqrt{\Delta t}$) have to be determined. For dE/dC, the change in concentration of the charge carrier is not directly measured but can be calculated under constant current.

$$dC = \frac{Idt_I}{FV} \quad 15$$

where V is the volume of the electrode and dt_I is the duration of the applied current. Assuming that dE/dC changes relatively slowly and thus can be interpolated by $\Delta E/\Delta C$,[1,6] Equation 7 can be rewritten as follows.

$$D = \frac{4}{\pi}\left(\frac{V}{A}\frac{\frac{\Delta E_{OC}}{\Delta t_I}}{\frac{dE}{d\sqrt{t}}}\right)^2 \quad 16$$

where ΔE_{OC} is the change in the open-circuit potential (OCP) from the rests before and after the current pulse, and Δt_I is the period of the current pulse (denoted as τ in the original paper[1]). It is worth noting that Equation 15 applies to the concentration of the entire electrode. In order to relate the measured electrode potential, which reflects the surface concentration, to the bulk concentration, the measurement should ideally be done when the concentration is uniform throughout the electrode. This is indicated by the fully relaxed electrode potential, i.e. $dE/dt = 0$, also known as the open-circuit condition. In practice, it takes long time to achieve equilibrium in the electrode, which is the reason for the substantial time consumption of GITT.[5]

$dE/d\sqrt{t}$ is the slope on the plot of E against $\sqrt{t}$. In the original GITT paper,[1] Equation 16 is further reduced by assuming that E is linear to $\sqrt{t}$ during the whole current pulse. However, this assumption is less likely to hold for electrode particles in a composite electrode since the duration for the semi-infinite diffusion condition, $t \ll L^2/D$, is reduced by the shorter L, compared to the bulk electrode used in the original paper. Two solutions to solve the issue are: 1) selecting only the data lying in the linear region on the E-$\sqrt{t}$ plot or 2) fitting the data with the full solution (Equation S3) to Fick's second law (method P3 and P5 in the reference, respectively).[4] In this work, we will proceed with the first solution and examine the effect of data selection on the GITT analysis.

2.4 Experimental execution of the ICI method

The change in the potential after the current has been switched off ($\Delta t = 0$) can be expressed as the following.

$$\Delta E(\Delta t) = E(\Delta t) - E_I = -IR - Ik\sqrt{\Delta t} \quad 17$$

where E_I is the potential right before the current is switched off, and R and k are termed internal resistance and diffusion resistance coefficient,

respectively.[10] R and k are acquired through the linear regression of ΔE against $\sqrt{\Delta t}$. For repetitive current pauses, the regression can be automated by a script in a common programing languages; R[23] has been used in this work.

Comparing Equation 14 and 17, it can be observed that

$$Ik = -\frac{dE}{d\sqrt{\Delta t}} = \frac{2I}{FA\sqrt{D\pi}}\frac{dE}{dC(0,t)} \tag{18}$$

which can be reorganized into the form of Equation 16 with Equation 15.

$$D = \frac{4}{\pi}\left(\frac{V}{A}\frac{\frac{dE_{OC}}{dt_I}}{Ik}\right)^2 \tag{19}$$

Without the relaxation step, dE_{OC}/dt_I, can be 1) obtained from existing OCP data of the electrode material or 2) approximated by the slope of iR-corrected pseudo-OCP. The iR-drop and pseudo-OCP, referring to the measured potential under low constant current,[5] are readily available in the ICI analysis. From two neighboring current interruptions, the change in OCP can be approximated by the change in $E(\Delta t=0)$, which is the potential right before the current pause subtracting the iR-drop, as shown in Equation 17. The validity of using $\Delta[E(\Delta t=0)]/\Delta t_I$ as dE_{OC}/dt_I will be examined in Section 3.

2.5 Experimental method

Two three-electrode half-cells, termed cells 1 and 2, were made for the validation of the theoretical derivation. The working electrode (⌀13 mm) was a tape-cast composite electrode consisting of 90 wt% NMC811 powder (Customcells Itzehoe GmbH), 5 wt% of carbon black (Super C65, Imerys) and 5 wt% poly(vinylidene difluoride) (PVdF, Solvay), whose fabrication procedure can be found in the previous work.[24] According to the supplier, the NMC811 particles have a median diameter of 4 μm and specific surface area of 1.5 m^2 g^{-1}, determined by the Brunauer–Emmett–Teller (BET) analysis of the nitrogen adsorption isotherm. The specific volume was calculated from the molecular mass and the previously reported (rhombohedral) unit cell parameters obtained through X-ray diffraction (XRD) to be 0.63056 cm^3 g^{-1}.[24] The areal loadings of NMC811 were 2.11 and 2.13 mg cm^{-2} in cells 1 and 2, respectively. Both the counter (⌀15 mm) and reference electrodes (ring with inner and outer diameters of 16 and 22 mm, respectively) were metallic lithium (Cyprus Foote Mineral, 125 µm thick). The reference electrode was placed between the

working and counter electrodes with separators (Celgard® 2325) on both sides according to a previously reported cell geometry.[11] The cells were assembled in an Ar-filled glove box with 1 M $LiPF_6$ in a mixture of ethylene carbonate/diethylene carbonate (EC/DEC 1:1 by volume, Solvionic, purity: 99.9%) as the electrolyte and sealed in pouch bag material. Assembled cells were rested for 12 hours before 3 pre-cycles at 20 mA g^{-1} between 3.0 and 4.3 V. Electrochemical tests were carried out using a Biologic MPG 2.

A modified GITT protocol was designed here to compare the GITT, ICI and EIS at the same SoC, which is schematically shown in Figure 1. A constant current of 20 mA g^{-1} (corresponding to C/10, where C is here defined as 200 mA g^{-1} for NMC811) was applied for 10 minutes, which was followed by a 1-hour rest. During the first minute of the rest, potential was recorded every 0.1 second for the ICI analysis. After the rest, an EIS measurement was performed from 20 kHz to 10 mHz with an amplitude of 10 mV. Another 10-minute rest followed the EIS measurement before the next current pulse. The modified GITT protocol was applied between 3.0 and 4.3 V for two cycles. In the second discharge, the cutoff was lowered to 2.0 and 2.5 V for cell 1 and 2, respectively. For both GITT and ICI analysis, the electrode volume and area were approximated by the volume and surface area of the NMC particles stated above. The BET-surface area may differ from the electrochemically active surface area. However, the objective of this work is to compare the GITT and ICI method, both of which are equally affected by this factor. The impedance spectra, where a Warburg element is present, were fitted to the equivalent circuit model in Figure S2 by a modified Levenberg-Marquardt algorithm provided by the “minpack.lm” package in the R-programming language.[25]

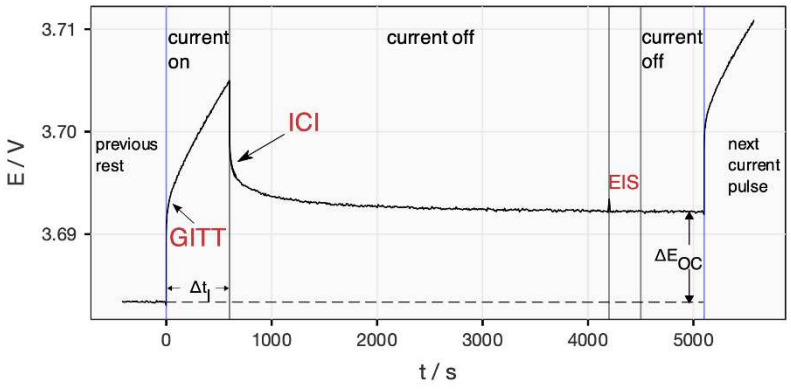

Figure 1. Electrode potential (E) plotted against time (t) during a current pulse (I = 20 mA g^{-1}) and a rest period (I = 0) of the modified GITT program used in this work for the comparison of the results from the GITT, ICI method and EIS. Note that the long rest period is not necessary for the ICI method. It is done in this manner here for the comparison between the three

methods.

After the above-described test, the cells went on to be cycled with the standard ICI protocol. Both cells were charged to 4.3 V and discharged to 3 V at a constant current of 20 mA g^{-1}. A 10-second current interruption every 5 and 15 minutes was introduced to cells 1 and 2, respectively. During the 57th discharge of cell 1, an operando XRD experiment was performed on the cell as it was charged up to 4.3 V and subsequently discharged to 3.7 V at 20 mA g^{-1} with a 10-second current interruption every 5 minutes, as in the previous cycles. Patterns were recorded by a STOE STADI P diffractometer in transmission setup with monochromatic Cu-$K_{\alpha 1}$ radiation every 15 minutes using a Dectris Mythen2 1K detector setup. Rietveld refinements[26,27] were performed against the XRD data using the Topas-Academic software (V6).[28] Further details of the refinements and the results are provided in the SI (Section 5).

3 Results and Discussion

Since cells 1 and 2 are identical and thus show similar behaviors in both cycles of the modified GITT protocol, the results of cell 1 in first cycle are discussed in detail while the rest is presented in the SI.

As shown in Equations 7, 16 and 19, to derive the diffusion coefficient, two measurements are required: $dE/d\sqrt{t}$ during semi-infinite diffusion and the slope of OCP. Therefore, the following text will first compare the two values obtained by the GITT and ICI method. Then, the diffusion coefficients calculated from the two methods will be presented. The data acquired during the current pulses and the rest periods are analyzed by the GITT and ICI methods, respectively, as indicated in Figure 1. For the GITT, two data selection intervals, 5–40 and 50–150 s, were utilized because they contain the linear region of the E-$\sqrt{t}$ plot above and below 3.7 V, respectively. An example of each case is plotted in Figure S1. Since more than 75% of the capacity of NMC811 is above 3.7 V, the GITT results in the following text are for clarity derived from the 5–40 s interval while results from both intervals can be found for both cells in the SI. For the ICI method, the interval was chosen to be 0.2–5 s for the same criteria applied on the data during the rest periods.

Figure 2 displays the k values, which are $dE/d\sqrt{t}$ normalized by the current (Equation 18) from GITT and ICI, and the Warburg coefficients (σ) multiplied by $\sqrt{8/\pi}$ from EIS fittings. This linear relationship of $k = \sigma\sqrt{8/\pi}$ has been demonstrated in previous work.[10] Above 3.8 V, the k values determined by ICI

and GITT are close to each other, which confirms the theoretical derivation in section 2.2 and is corroborated by the EIS results. During discharge, the *k* values obtained from EIS are slightly higher than those from the GITT and ICI measurements, while the latter two remain close to each other. In Figure S5, a statistical analysis on the relative difference between the *k* values from the GITT and ICI methods is exhibited. The close-to-zero average indicates that no systematic error appears, while the standard deviation being at 24% is promising when considering the large range of the GITT measurements of this same material in the literature, which scatters over two orders of magnitude.[29]

Below 3.7 V, the linear region on the E-$\sqrt{t}$ plots of the GITT measurements shifts to 50–150 s, as demonstrated in Figure S1, which indicates an increase in the time constant of the charge-transfer related process. This phenomenon is confirmed by the expansion of the second semi-circle on impedance spectra (Figure S4), which do not show a Warburg element within the frequency range (20 kHz–10 mHz) and thus cannot render *k* values below 3.7 V. The increase in charge transfer resistance represented by the enlarged semi-circle has been reported for NMC111 ($LiNi_{0.33}Mn_{0.33}Co_{0.33}O_2$) at low SoC, which pushes the Warburg element to frequencies lower than 10 mHz.[2,18] This indicates that neither the EIS above 10 mHz, GITT with 5–40 s data selection interval nor the ICI method accurately characterize the diffusion process below 3.7 V. Between 3.7 and 3.8 V, a mismatch between the GITT and ICI methods can be observed during charging, but not during discharging. The difference can be an effect of the varying charge transfer resistance and different data selection time intervals of the two techniques. In summary, Figure 2 illustrates the consistency of EIS, GITT and ICI method within their respective limitations.

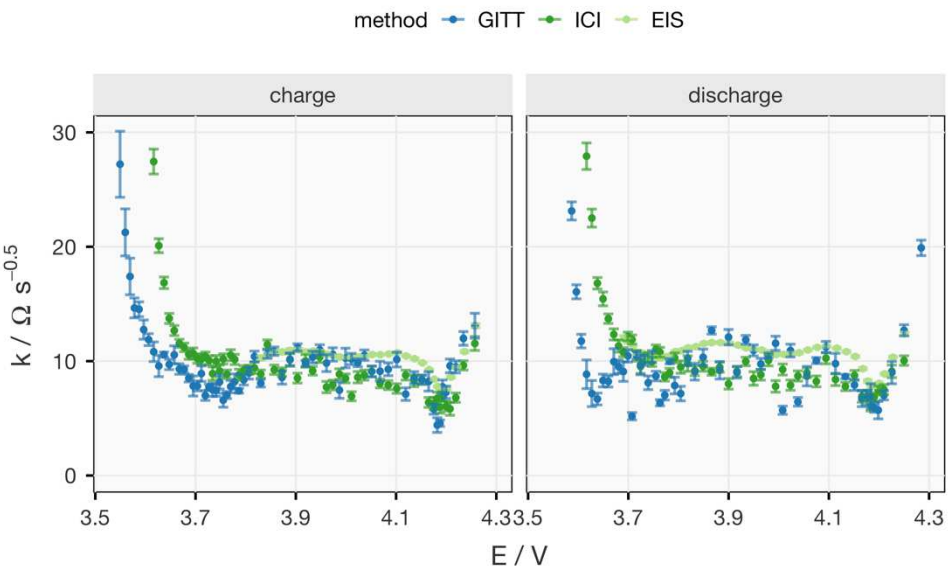

Figure 2. The diffusion resistance coefficient (k) in NMC811(D) in cell 1 at various OCP of the electrode (E) against Li/Li+ derived from the GITT with data selection interval 5–40 s, the ICI method and the EIS fitting ($k = \sigma\sqrt{8/\pi}$, σ: Warburg coefficient). The maximum of the *y*-axis is set to 30 Ω $s^{-0.5}$ to show the differences of the data above 3.7 V. Due to a technical issue, the spectra below 3.8 V in the first charge were not properly collected, but it was solved afterwards. The analysis of the difference between the values derived from the GITT and ICI methods can be found in Figure S5.

The other quantity experimentally determined in these methods used in the calculation of the diffusion coefficient (Equations 16 and 19) is the OCP slope. Figure 3 presents a comparison between the slopes of the OCP obtained from the relaxed potential at the end of the rest period in the GITT protocol and the iR-corrected pseudo-OCP in the ICI analysis. The difference between the values from two methods are minimal above 3.65 V, which is confirmed by the close-to-zero average and minimal standard deviation (0.086) of the relative difference in Figure S6. The deviation at low SoC is presumably linked to the high resistance discussed above, which interferes with the resistance determination of the ICI method. Nevertheless, the good agreement between the slopes of OCP and iR-corrected pseudo-OCP in most SoC intervals indicates that the ICI method alone can deliver the required electrochemical parameters for the calculation of the diffusion coefficient. By skipping the time-consuming relaxation periods, the ICI method can save around 90% of the time spent on common GITT protocols, such as the one used in this work.

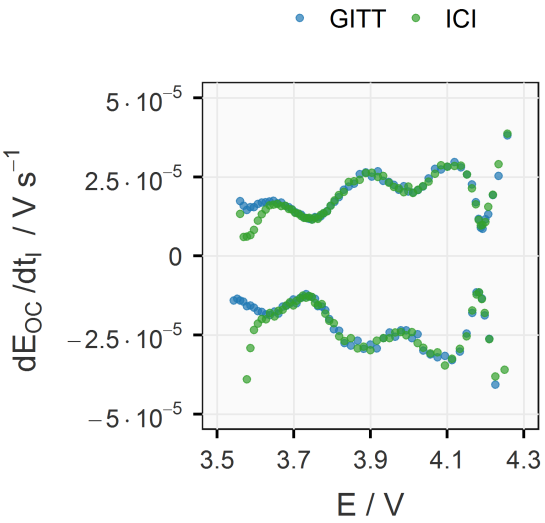

Figure 3. The slope of the OCP (dE_{OC}/dt_I) obtained from the relaxed potentials at the end of each rest period (GITT) is compared with the slope of the potential under constant-current load subtracting the iR-drop derived from the ICI method ($\Delta[E(\Delta t=0)]/\Delta t_I$, marked as ICI). The analysis of the difference between the values derived from the GITT and ICI methods can be found in Figure S6.

With both experimental inputs verified, the diffusion coefficients of Li^+ in NMC811 at various SoC obtained by the GITT and ICI method are exhibited in Figure 4. Overall, the results from the three analyses are close to each other and previously reported Li^+ diffusion coefficients in NMC811.[5,30] Above 3.8 V, the match is close for the values from the GITT and the ICI method. This is expected since the $dE/d\sqrt{t}$ values derived from both GITT and ICI method are in good agreement above 3.8 V in Figure 2 and the slopes of OCP from both methods are basically the same above 3.65 V in Figure 3. Below 3.7 V, differences between the two analyses are obvious since neither method characterizes the diffusion process, as discussed above. Between 3.7 and 3.8 V, the match during discharge and the slight mismatch during charge are also expected from the comparison in Figure 2. As expected from the differences of k and dE_{OC}/dt_I from both methods in Figure S5 and S6, the average relative difference in Li^+ diffusion coefficient is also close to zero, 0.071, and the standard deviation is 41%, which is actually small compared to the wide-spreading reported values in the literature, as discussed above. Including the results from cell 2 in Figure S9, it can be concluded that both methods generally agree with each other above 3.7 V, while a more consistent match can be found above 3.8 V. This demonstrates the validity of the ICI method as an efficient alternative to GITT.

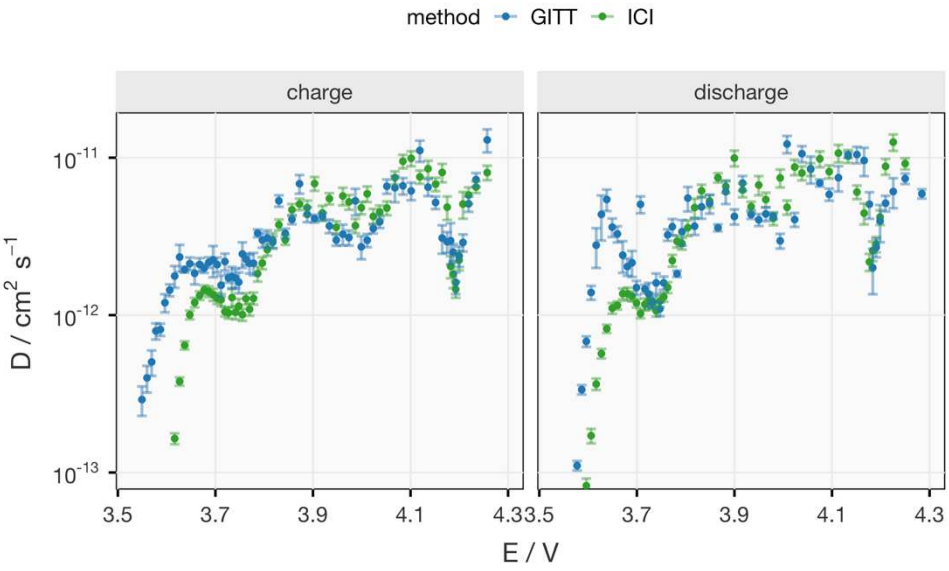

Figure 4. The Li-ion diffusion coefficient in NMC811(D) in cell 1 at various OCP of the electrode (E) against Li/Li$^+$ derived from the GITT with data selection interval 5–40 s and the ICI method. The minimum of the *y*-axis is set to 10^{-13} cm^2 s^{-1} to show the differences of the data above 3.7 V. The analysis of the difference between the values derived from the GITT and ICI methods can be found in Figure S7.

Other valuable information provided by the ICI method is the internal resistance (*R*), as shown in Figure 5. *R* values derived from the iR-drop in the GITT and ICI method are compared with the sum of R0, R1 and R2 from EIS (Figure S2). The results from ICI and EIS are almost identical across the whole range of SoC. The GITT yields similar *R* values during discharge but larger values upon charging. Nonetheless, all methods confirm the high internal resistance below 3.7 V, which changes the linear region of E-$\sqrt{t}$ plots, as discussed above. The internal resistance has been reported to be an important indicator for ageing of NMC811[31] and utilized for detecting Li-plating in commercial Li-ion cells.[13]

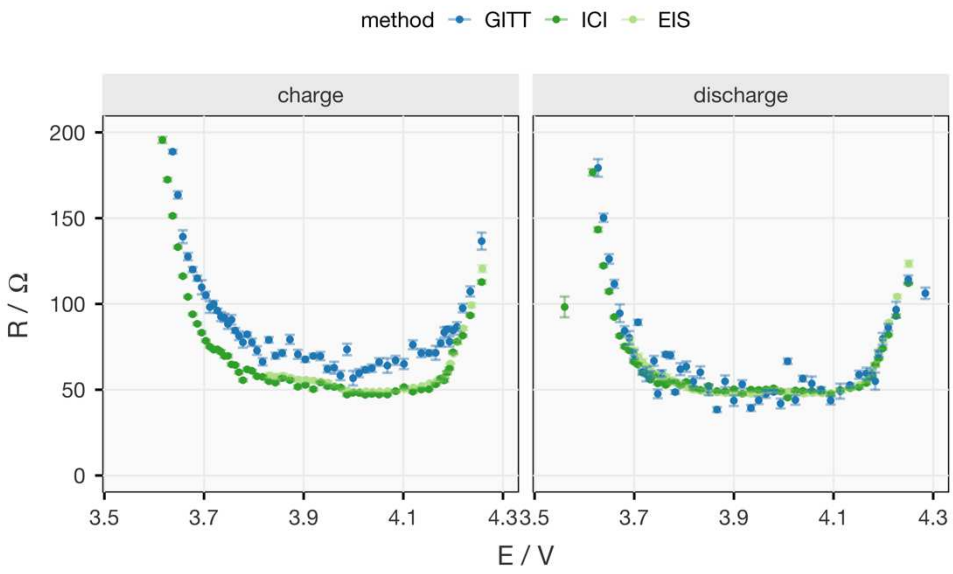

Figure 5. The internal resistance (R) of NMC811 in cell 1 at various OCP of the electrode (E) against Li/Li+ derived from the GITT with data selection interval 5–40 s, the ICI method and the EIS fitting (R0+R1+R2 in the equivalent circuit model in Figure S2). The maximum of y-axis is set to 200 Ω to show the differences of the data above 3.7 V.

The value of the ICI method's efficiency is illustrated by the results in Figure 6, which show the change in Li-ion diffusion coefficient and internal resistance over more than 50 cycles of constant-current charge and discharge. While the internal resistance increases more uniformly in all SoC, a clear decrease in the Li-ion diffusion coefficient can be observed above 4.2 V. The rate of decrease is higher in the first 15 cycles than in the following cycles. This SoC range, 4.2–4.3 V, corresponds to the drastic shrinkage of the *c* lattice parameter of the rhombohedral ($R\bar{3}m$) unit cell, which has been reported in previous *operando* XRD studies of NMC811.[24,32–34] To confirm the correlation between the decreasing Li-ion diffusivity observed here and the microstructural evolution of NMC811, a combination of *operando* XRD and the ICI method was carried out after the 56th galvanostatic cycle.

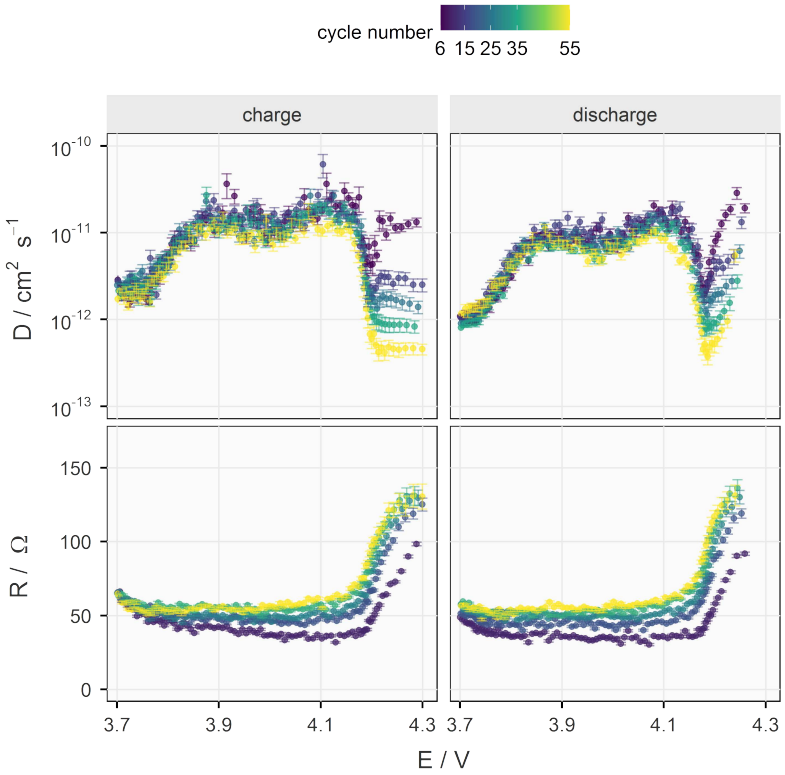

Figure 6. The Li-ion diffusion coefficient in NMC811(D) and internal resistance (R) of cell 1 at various electrode potential (E) against Li/Li^+ derived by the ICI method in cycle 6, 15, 25, 35 and 55. Note that the electrode potential here is obtained while cycling, not the OCP. Only values with $E \geq 3.7$ V, where the ICI method is applicable as discussed above, are shown.

The *operando* XRD experiment coupled with the ICI method was performed on cell 1 after 56 cycles. As depicted in Figure 7, when the 003 reflection ($R\bar{3}m$) shifts to higher 2θ values, the diffusion coefficient drops over an order of magnitude and the internal resistance tripled. The shift of the 003 reflection starts at 4.1 V and accelerates at 4.2 V, which coincides with the start of the increase in internal resistance and the decrease in diffusion coefficient, respectively. The reverse can be observed during discharge. In addition, by comparing the patterns taken above 4.2 V with a previous *operando* XRD study on the same material in the first cycle,[24] it can be observed that in the degraded cell here, the 003 reflection is composed of two rhombohedral phases with dissimilar *c* lattice parameters (Figure S16). The exact mechanism for this phase separation is still debated, but most models attribute this to the ramifications of the formation of the degraded rock salt phase.[32,35,36] Nevertheless, it is shown here that the ICI method can be easily combined with

operando XRD and track the diffusion coefficient and internal resistance in real time, which constitutes a valuable method for further studies of the degradation mechanisms of this and other materials.

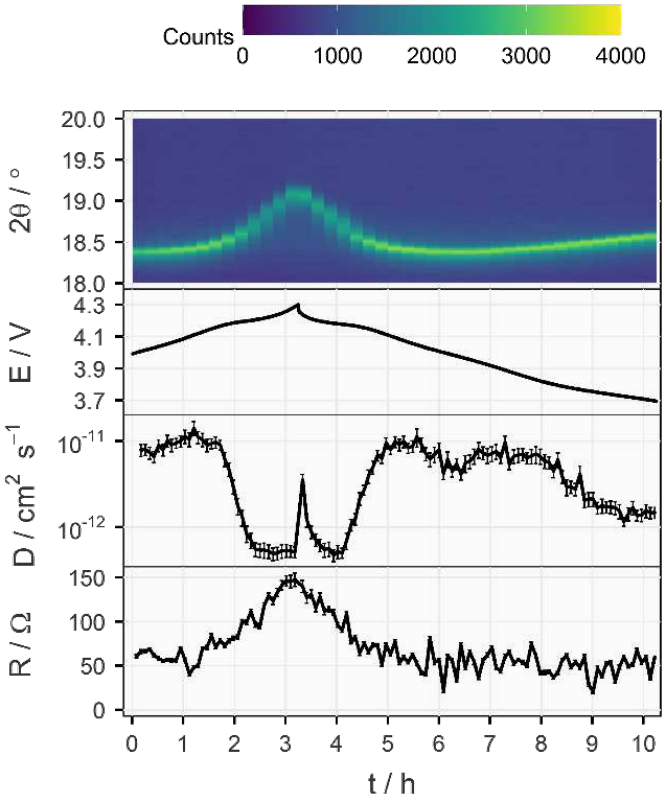

Figure 7. The evolution of the 003 (first panel) reflections (Cu-Kα_1) as a heat map, electrode potential (E), Li-ion diffusion coefficient in NMC811 (D) and the internal resistance (R) from the combination of operando XRD and the ICI method conducted on cell 1 after 56 galvanostatic cycles between 3.0 and 4.3 V and the 57th charge to 4.0 V. The incomplete cycle does not affect the observation of the correlation between the Li-ion diffusivity and the structural change above 4.2 V.

4 Conclusions

This work establishes the theoretical foundation and experimental validation for the application of the ICI method as an efficient alternative to GITT. Provided that 1) the diffusion process under investigation exhibits the semi-infinite diffusion behavior within the maximum time allowed for the current interruption and that 2) the pseudo-OCP slope is a good approximation of the true OCP slope, the ICI method can yield the diffusion coefficient with a much shorter experimental time. In the case of our validation experiment with NMC811, more than 90% of the time required for a typical GITT experiment

can be saved. Moreover, the internal resistance and diffusion resistance coefficient (or equivalently, the Warburg coefficient) determined by the ICI method are also verified by EIS for NMC811. The efficient determination of diffusivity and resistance unlocks new applications which GITT and EIS are deemed too time- or resource-consuming, such as online cell parameterization for adaptive charging protocol and simultaneous observation of *operando* spectro-/diffractometry and electrochemical impedance/resistance. When exemplified by a combination of *operando* XRD and the ICI method, the rapid decrease of the Li-ion diffusion coefficient above 4.2 V over cycling could be correlated to the increasing irreversibility of the contraction and elongation of the *c* lattice parameter of the NMC structure. To our knowledge, it is the first report of concurrent characterization of the crystal structure and the Li^+ diffusion coefficient.

References

(1) Weppner, W.; Huggins, R. A. Determination of the Kinetic Parameters of Mixed-Conducting Electrodes and Application to the System Li3Sb. *J. Electrochem. Soc.* **1977**, *124* (10), 1569–1578.

(2) Shaju, K. M.; Subba Rao, G. V.; Chowdari, B. V. R. Influence of Li-Ion Kinetics in the Cathodic Performance of Layered Li(Ni[Sub 1/3]Co[Sub 1/3]Mn[Sub 1/3])O[Sub 2]. *J. Electrochem. Soc.* **2004**, *151* (9), A1324.

(3) Dees, D. W.; Kawauchi, S.; Abraham, D. P.; Prakash, J. Analysis of the Galvanostatic Intermittent Titration Technique (GITT) as Applied to a Lithium-Ion Porous Electrode. *J. Power Sources* **2009**, *189* (1), 263–268.

(4) Nickol, A.; Schied, T.; Heubner, C.; Schneider, M.; Michaelis, A.; Bobeth, M.; Cuniberti, G. GITT Analysis of Lithium Insertion Cathodes for Determining the Lithium Diffusion Coefficient at Low Temperature: Challenges and Pitfalls. *J. Electrochem. Soc.* **2020**, *167* (9), 090546.

(5) Chen, C.-H.; Brosa Planella, F.; O'Regan, K.; Gastol, D.; Widanage, W. D.; Kendrick, E. Development of Experimental Techniques for Parameterization of Multi-Scale Lithium-Ion Battery Models. *J. Electrochem. Soc.* **2020**, *167* (8), 080534.

(6) Wen, C. J.; Boukamp, B. A.; Huggins, R. A.; Weppner, W. Thermodynamic and Mass Transport Properties of "LiAl." *J. Electrochem. Soc.* **1979**, *126* (12), 2258.

(7) Tang, X.-C.; Pan, C.-Y.; He, L.-P.; Li, L.-Q.; Chen, Z.-Z. A Novel Technique Based on the Ratio of Potentio-Charge Capacity to

Galvano-Charge Capacity (RPG) for Determination of the Diffusion Coefficient of Intercalary Species within Insertion-Host Materials: Theories and Experiments. *Electrochim. Acta* **2004**, *49* (19), 3113–3119.

(8) Lacey, M. J.; Edström, K.; Brandell, D. Visualising the Problems with Balancing Lithium–Sulfur Batteries by “Mapping” Internal Resistance. *Chem. Commun.* **2015**, *51* (92), 16502–16505.

(9) Lacey, M. J. Influence of the Electrolyte on the Internal Resistance of Lithium–Sulfur Batteries Studied with an Intermittent Current Interruption Method. *ChemElectroChem* **2017**, *4* (8), 1997–2004.

(10) Chien, Y.-C.; Menon, A. S.; Brant, W. R.; Brandell, D.; Lacey, M. J. Simultaneous Monitoring of Crystalline Active Materials and Resistance Evolution in Lithium–Sulfur Batteries. *J. Am. Chem. Soc.* **2020**, *142* (3), 1449–1456.

(11) Aktekin, B.; Lacey, M. J.; Nordh, T.; Younesi, R.; Tengstedt, C.; Zipprich, W.; Brandell, D.; Edström, K. Understanding the Capacity Loss in LiNi 0.5 Mn 1.5 O 4 –Li 4 Ti 5 O 12 Lithium-Ion Cells at Ambient and Elevated Temperatures. *J. Phys. Chem. C* **2018**, *122* (21), 11234–11248.

(12) Hernández, G.; Naylor, A. J.; Chien, Y.-C.; Brandell, D.; Mindemark, J.; Edström, K. Elimination of Fluorination: The Influence of Fluorine-Free Electrolytes on the Performance of LiNi 1/3 Mn 1/3 Co 1/3 O 2 /Silicon–Graphite Li-Ion Battery Cells. *ACS Sustain. Chem. Eng.* **2020**, *8* (27), 10041–10052.

(13) Koleti, U. R.; Dinh, T. Q.; Marco, J. A New On-Line Method for Lithium Plating Detection in Lithium-Ion Batteries. *J. Power Sources* **2020**, *451*, 227798.

(14) de Levie, R. On Porous Electrodes in Electrolyte Solutions. *Electrochim. Acta* **1963**, *8* (10), 751–780.

(15) Lasia, A. Impedance of Porous Electrodes. *J. Electroanal. Chem.* **1995**, *397* (1–2), 27–33.

(16) Bard, A. J.; Faulkner, L. R. *Electrochemical Methods: Fundamentals and Applications*, 2nd ed.; Wiley, 2000.

(17) Lasia, A. *Electrochemical Impedance Spectroscopy and Its Applications*; Springer New York: New York, NY, 2014.

(18) Charbonneau, V.; Lasia, A.; Brisard, G. Impedance Studies of Li+ Diffusion in Nickel Manganese Cobalt Oxide (NMC) during Charge/Discharge Cycles. *J. Electroanal. Chem.* **2020**, *875*, 113944.

(19) Carslaw, H. S.; Jaeger, J. C. *Conduction of Heat in Solids*, 2nd ed.; Oxford science publications; Clarendon: Oxford, 1986.

(20) Liu, S. An Analytical Solution to Li/Li+ Insertion into a Porous Electrode. *Solid State Ionics* **2006**, *177* (1–2), 53–58.
(21) Subramanian, V. R.; White, R. E. New Separation of Variables Method for Composite Electrodes with Galvanostatic Boundary Conditions. *J. Power Sources* **2001**, *96* (2), 385–395.
(22) Subramanian, V. R.; Ritter, J. A.; White, R. E. Approximate Solutions for Galvanostatic Discharge of Spherical Particles I. Constant Diffusion Coefficient. *J. Electrochem. Soc.* **2001**, *148* (11), E444.
(23) R Core Team. R: A Language and Environment for Statistical Computing https://www.r-project.org/.
(24) Liu, H.; Naylor, A. J.; Menon, A. S.; Brant, W. R.; Edström, K.; Younesi, R. Understanding the Roles of Tris(Trimethylsilyl) Phosphite (TMSPi) in LiNi 0.8 Mn 0.1 Co 0.1 O 2 (NMC811)/Silicon–Graphite (Si–Gr) Lithium-Ion Batteries. *Adv. Mater. Interfaces* **2020**, *7* (15), 2000277.
(25) Elzhov, T. V.; Mullen, K. M.; Spiess, A.-N.; Bolker, B. Minpack.Lm: R Interface to the Levenberg-Marquardt Nonlinear Least-Squares Algorithm Found in MINPACK, Plus Support for Bounds. 2016.
(26) Rietveld, H. M. Line Profiles of Neutron Powder-Diffraction Peaks for Structure Refinement. *Acta Crystallogr.* **1967**, *22* (1), 151–152.
(27) Rietveld, H. M. A Profile Refinement Method for Nuclear and Magnetic Structures. *J. Appl. Crystallogr.* **1969**, *2* (2), 65–71.
(28) Coelho, A. A. TOPAS and TOPAS-Academic: An Optimization Program Integrating Computer Algebra and Crystallographic Objects Written in C++: An. *J. Appl. Crystallogr.* **2018**, *51* (1), 210–218.
(29) Chouchane, M.; Primo, E. N.; Franco, A. A. Mesoscale Effects in the Extraction of the Solid-State Lithium Diffusion Coefficient Values of Battery Active Materials: Physical Insights from 3D Modeling. *J. Phys. Chem. Lett.* **2020**, *11* (7), 2775–2780.
(30) Hu, J.; Wu, B.; Cao, X.; Bi, Y.; Chae, S.; Niu, C.; Xiao, B.; Tao, J.; Zhang, J.; Xiao, J. Evolution of the Rate-Limiting Step: From Thin Film to Thick Ni-Rich Cathodes. *J. Power Sources* **2020**, *454*, 227966.
(31) Strehle, B.; Friedrich, F.; Gasteiger, H. A. A Comparative Study of Structural Changes during Long-Term Cycling of NCM-811 at Ambient and Elevated Temperatures. *J. Electrochem. Soc.* **2021**, *168* (5), 050512.
(32) Li, J.; Downie, L. E.; Ma, L.; Qiu, W.; Dahn, J. R. Study of the Failure Mechanisms of LiNi 0.8 Mn 0.1 Co 0.1 O 2 Cathode Material for Lithium Ion Batteries. *J. Electrochem. Soc.* **2015**, *162* (7), A1401–A1408.

(33) Märker, K.; Reeves, P. J.; Xu, C.; Griffith, K. J.; Grey, C. P. Evolution of Structure and Lithium Dynamics in LiNi 0.8 Mn 0.1 Co 0.1 O 2 (NMC811) Cathodes during Electrochemical Cycling. *Chem. Mater.* **2019**, *31* (7), 2545–2554.

(34) Xu, C.; Märker, K.; Lee, J.; Mahadevegowda, A.; Reeves, P. J.; Day, S. J.; Groh, M. F.; Emge, S. P.; Ducati, C.; Layla Mehdi, B.; Tang, C. C.; Grey, C. P. Bulk Fatigue Induced by Surface Reconstruction in Layered Ni-Rich Cathodes for Li-Ion Batteries. *Nat. Mater.* **2021**, *20* (1), 84–92.

(35) Xu, C.; Reeves, P. J.; Jacquet, Q.; Grey, C. P. Phase Behavior during Electrochemical Cycling of Ni-Rich Cathode Materials for Li-Ion Batteries. *Adv. Energy Mater.* **2021**, *11* (7), 1–12.

(36) Friedrich, F.; Strehle, B.; Freiberg, A. T. S.; Kleiner, K.; Day, S. J.; Erk, C.; Piana, M.; Gasteiger, H. A. Editors' Choice—Capacity Fading Mechanisms of NCM-811 Cathodes in Lithium-Ion Batteries Studied by X-Ray Diffraction and Other Diagnostics. *J. Electrochem. Soc.* **2019**, *166* (15), A3760–A3774.

Supplementary Files

This is a list of supplementary files associated with this preprint. Click to download.

- SI.pdf